frontiers

Temporal variability of spectral Granger causality from neural networks (EEGs) during sleep: a time-frequency approach

Louis Almairac [1], **Alexandre André** [1], **Matthieu Pascal** [1], **Alexandre Guillet**[2], **Pierre Argoul**[3] **and Francoise Argoul**[4]

[1] *Département IMI Ingénierie Mathématique et Informatique, Ecole Nationale des Ponts et Chaussées, 77454 Marne la Vallée, FRANCE*
[2] *Max Planck Institute for the Physics of Complex Systems, Dresden, GERMANY*
[3] *LVMT, Ecole Nationale des Ponts et Chaussées, Université Gustave Eiffel, 77454 Marne la Vallée, FRANCE*
[4] *LOMA, CNRS UMR5798, Université de Bordeaux, Talence, FRANCE*

Correspondence*:
francoise.argoul@u-bordeaux.fr

ABSTRACT

Introduction Since its emergence, the notion of causality was linked to conditional dependence measures and constructed from linear decompositions (autoregressive) of variables on their previous occurrences. A signal Y is said to be causal for another signal X ($Y \rightarrow X$) in the Granger sense, if past values of Y contain information (innovations) that could better predict X than solely the information contained in past values of X. A key assumption of Granger causality approaches is that the data sample is stationary.

Over the past decade, neurophysiological recordings (e.g. electroencephalograms (EEGs)) and high-resolution neuroimaging techniques have provided large amounts of multivariate data and have opened a whole new field of physiological neural networks. Granger causality was extensively utilised as a statistical method for deciphering neural interactions and their causality, however, regression methods were often time-consuming when applied to high-order VAR models. Moreover, they were more likely to include errors and misinterpretations when dealing with non-stationary signals. In part, because they do not consider temporal changes in inter-signal causality. Spectral causality was also proposed to extract the frequency distributions of causality.

Methods: We propose here a time-frequency approach of causality, based on wavelet transforms, to analyze synthetic and real signals (electroencephalographic) recorded during sleep. This original method is compared with more traditional temporal and spectral causality, to highlight its wide interest. We apply this method to analyze neural network interactions from EEG recordings during sleep.

Results: We show that the temporal and frequency localizations of the coupling of distant cortex sites during sleep are important markers for understanding the stability of the different sleep phases. Examining the transitions from distinct sleep phases such as N2$\rightarrow$ N3, N2$\rightarrow$REM, N2$\rightarrow$W, we observe that interbrain correlations can undergo significant changes, pointing out

the interest of time-frequency Granger computation for estimating transitory phases (temporal extension, frequency band shift).

Discussion: This work may also provide a new perspective on the origin of apnoea (obstructive or central) by incorporating ECG, O_2 saturation and respiratory signals into this non-parametric time-frequency approach to Granger causality. Recent clinical studies have indicated that both central and obstructive apnoea may play a role in the progression of sleep disorders.

Keywords: Granger causality; directional, instantaneous causalities; electroencephalogram, neural networks, sleep phases

1 INTRODUCTION

The notion of causality takes its roots from very ancient times, from human beings' observation of the cyclic nature of life and natural events. Inspired from the work of Wiener, Clive Granger Granger ((1969)) elaborated a mathematical framework to describe a form of causal relationship between two variables $X(t)$ and $Y(t)$ where the past observation of Y improves the prediction of the current state of X (and *vice-versa*).

Causality inference via GC has been widely applied in different areas of science, and more recently to physiological functional networks of the brain using fMRI Havlicek et al. ((2010)); Liao et al. ((2010)), MEG Alves et al. ((2023)), and EEG Barrett et al. ((2012)); Seth et al. ((2015)). Alternative measures have been proposed, namely linear correlations Lynall et al. ((2010)), mutual information Piasini and Panzeri ((2019)), partial directed coherence Baccalá and Sameshima ((2001)), ordinary coherence Fries ((2005)), directed transfer function Kaminski and Blinowska ((1991)), spectral coherence Rocca et al. ((2014)), and transfer entropy Schreiber ((2000)); Vicente et al. ((2011)), although they may require more computational efforts, based on the estimation of probability density functions of one or more variables. However, Granger spectral causality, based on computation of probability density functions Geweke ((1981)); Chicharro ((2011)), has also been proposed. This rich variety of approaches for understanding causality and/or connectivity in brain networks points out the importance of this field Charleston-Villalobos et al. ((2023)). Granger, when introducing this causality had in mind that the real system he was studying could be modelled or approximated by parametric equations. He used autoregressive equations (AR) Granger ((1969)) which were further improved to autoregressive moving average models (ARMA). When the model parameters are chosen to give a best of a whole sequence of data samples (non-adaptive model) non stationary system cannot be described (which was the original Granger hypothesis). On the opposite, when the model parameters can be updated when new data samples are included in the analysis (adaptive models) non stationary cases.

The concept of causality is typically related to whether interventions on a source can have an effect on a given target, rather than whether observation of the source can help predict state transitions of the target. The latter concept is information transfer, whilst the former one is related to causality. The measurement of the Granger causality (GC) between variables may be done in both the time and the frequency domains, however most study focus on one of these methods specifically. To support the analysis of complex (multi-scale) and time-varying physiological networks, we propose here a time-frequency approach of causality, based on wavelet transforms, to analyze synthetic and real signals (electroencephalographic (EEG) neural network interactions) recorded during sleep. This original method will be compared with more traditional temporal and spectral causality, to highlight its wide interest. In the section 2 we describe the methods used in this work and their discuss their foundation, advantage or drawback compared to other methods. In section 4 we apply this method to two type of signals, numerical signals produced by auto-regressive

models, and EEG signals. Section 5 propose a discussion of the results of our computation and open new perspectives for future applications to neuroscience or more generally physiological networks modeling.

2 METHODS

2.1 EEG databases and signals pretreatments

2.1.1 EEG databases

The EEG signals were obtained from the public database of the PhysioNet Challenge 2018 (P2018C), 'You Snooze, You Win' (MGH Sleep Lab Database) Ghassemi et al. ((2018)); Goldberger et al. ((2000)). Data for this challenge were contributed by the Massachusetts General Hospital's (MGH) Computational Clinical Neurophysiology Laboratory (CCNL), and the Clinical Data Animation Laboratory (CDAC). The dataset includes 1,985 subjects which were monitored at an MGH sleep laboratory for the diagnosis of sleep disorders. The data were partitioned into balanced training (n = 994), and test sets (n = 989). This resource contains complete polysomnographic recordings of patients in a sleep clinic, allowing physiological activity to be monitored throughout the night. The sleep stages of the subjects were annotated by clinical staff at the MGH according to the American Academy of Sleep Medicine (AASM) manual for the scoring of sleep. More specifically, the following six sleep stages were annotated in 30 second contiguous intervals: wakefulness, stage 1, stage 2, stage 3, rapid eye movement (REM), and undefined.

The subjects had a variety of physiological signals recorded as they slept through the night including: electroencephalography (EEG), electrooculography (EOG), electromyography (EMG), electrocardiology (EKG), and oxygen saturation (SaO2). Excluding SaO2, all signals were sampled to 200 Hz and were measured in microvolts. For analytic convenience, SaO2 was resampled to 200 Hz, and is measured as a percentage.

Type	**Localisation**	**Sensors**	**Fonction / measure principle**
EEG	occipital lobe, median line, front of the skull	O1, O2, C3, C4, F3, F4	Measures of the electrical activity of the brain: - visual cortex (O1, O2) - motor (C3, C4) - frontal, attention (F3, F4)
EOG	Periocular region	E1, E2	Detection of eyes movements.
EMG	Under the chin	Chin1, Chin2	Measure of muscular tone.
ECG	Thorax	ECG	Measure of heart activity.
Respiration	Thorax, abdomen, nose/mouth	ABD, CHEST, AIRFLOW	Pressure or air flux sensors: capture respiration signals.
SaO_2	on finger or ear lobe	Pulse oxymeter	Optical sensor for O_2 saturation.

Table 1. Table of the different records of the P2018C

2.1.2 EEG pretreatment

Before further analysis, EEG raw signals undergo pre-processing to eliminate artefacts and isolate physiologically relevant components:

1. **Bandpass filtering (0.1–40 Hz)**: This digital filter allows only frequencies useful for neurophysiological signal analysis to be retained. It eliminates very slow variations (due to movement, position changes or baseline drifts) and attenuates high frequencies often associated with noise, such as muscle or electronic activity.

2. **50 Hz notch filtering**: A very narrow band-stop filter is applied around 50 Hz to suppress electrical noise, typically caused by mains power in hospital or urban environments. *Note:* Although the bandpass filter already attenuates most of the 50 Hz signal (the high cutoff frequency is set to 40 Hz), the notch is applied as a supplement to ensure complete elimination of residual electrical interference. This precaution is useful if the bandpass filter does not have a perfectly steep cutoff slope, or in the presence of persistent artefacts.

2.2 Time-frequency analysis

Time-frequency analysis, based on wavelet transform, was introduced in the second half of the twentieth century and applied to many scientific domains, from geophysics, fractals, mechanical systems, optics, accoustic, electrophysiology, cardiology, ...Grossmann and Morlet ((1984)); Carmona et al. ((1995, 1997, 1998)).

The wavelet transform of a finite energy signal $s(t) \in L^2(\mathbb{R})$ is defined as its inner product with shifted copies of an analyzing (mother) wavelet $\psi(t) \in L^1(\mathbb{R}) \cap L^2(\mathbb{R})$ Mallat and Peyré ((2009)); Torresani and Meyer ((1995)). The wavelet transform of a real signal s is defined from two parameters: a shift parameter $b \in \mathbb{R}$ and a scaling parameter $a \in \mathbb{R}_+^*$:

$$\mathcal{W}_\psi[s](a,b) = \left\langle s, \psi_{a,b} \right\rangle = a^{-\frac{1}{p}} \int_{-\infty}^{+\infty} s(t)\psi^* \left(\frac{t-b}{a} \right) dt, \tag{1}$$

ψ^* is the complex conjugate of the analyzing wavelet ψ, p defines the convention of normalization of the wavelet: $p = 2$ for a $L^2(\mathbb{R})$ norm (constant energy for the wavelet) and $p = 1$ for a $L^1(\mathbb{R})$ norm (constant magnitude for the wavelet).

In the sequel, we use the norm $L^2(\mathbb{R})$ norm ($p = 2$) for the wavelet because it preserves the energy of the signal when scaling the time. Hence the wavelet transform reads:

$$\mathcal{W}_\psi[s](a,b) = \left\langle s, \psi_{a,b} \right\rangle = a^{-\frac{1}{2}} \int_{-\infty}^{+\infty} s(t)\psi^* \left(\frac{t-b}{a} \right) dt, \tag{2}$$

In the frequency domain this wavelet transform reads:

$$\mathcal{W}_\psi[s](a,b) = a^{\frac{1}{2}} \int_{-\infty}^{+\infty} \hat{s}(f)\ \hat{\psi}^*(af)\, e^{i2\pi f b} df\ . \tag{3}$$

This time-scale representation is well suited for non-stationary signals since it localizes the analysis around the time b and operates a band-pass filtering scaled by the parameter a. Importantly, a can be sampled arbitrarily, on linear or logarithmic scales. For noisy or singular signals a logarithmic scale is more appropriate. For rhythmic signals, complex analysing wavelets are preferred, with linear scale. The characteristic frequency of the wavelet f_0 corresponds to the local maximum of $\hat{\psi(f)}$. The time-scale analysis of Eq. (1) can be turned to a time-frequency analysis by introducing a frequency parameter $f_a = f_0/a$.

The admissibility condition for an analysing wavelet $\psi \in L^1(\mathbb{R}) \cap L^2(\mathbb{R})$ establishes that the number c_ψ

$$c_\psi = \int_0^{+\infty} |\hat{\psi}(af)|^2\ \frac{\mathrm{d}a}{a}\ , \tag{4}$$

must be finite, nonzero and independent of $f \in \mathbb{R}^+$.

If this admissibility condition is fulfilled then every signal $s \in L^2(\mathbb{R})$ can be reconstructed from the convergent integral **?**:

$$s(t) = \frac{2}{c_\psi} \Re \int_{-\infty}^{+\infty} \int_0^{\infty} \mathcal{W}_\psi[s]\,(a,b)\,\psi\left(\frac{t-b}{a}\right) \frac{\mathrm{d}a\mathrm{d}b}{a^{\frac{3}{2}}}\ , \tag{5}$$

Because the analysing wavelet is scale invariant (under dilations), its quality factor Q is a fixed parameter for the analysis. Referring to the conventional frequency analysis of constant-Q filters, Le and Argoul ((2004)) introduced a parameter Q_m, called "quality factor", for the time-frequency resolution of the CWT. This quality factor Q_m is defined as the ratio of the mean value $\bar{f}_\psi$ (in terms of the root mean squares with L_2 norm) over two times the standard deviation Δf_ψ of $\hat{\psi}$.

Similarly to the reconstruction integral Eq. (5), the energy of a square integrable signal $s \in L^2(\mathbb{R})$ can be computed from its wavelet transform as:

$$\int_{-\infty}^{+\infty} |s(t)|^2 \mathrm{d}t = \frac{2}{c_\psi} \int_{-\infty}^{+\infty} \int_0^{\infty} |\mathcal{W}_\psi[s]\,(a,b)\,|^2 \frac{\mathrm{d}a\mathrm{d}b}{a^2}\ . \tag{6}$$

The square of the modulus of the wavelet transform (suitably normalised) can therefore be interpreted as time-scale or time-frequency energy density.

Among the simplest complex wavelets we have the so-called Cauchy (or Paul) and the Morlet wavelets, which have been intensively used in quantum mechanics, analytic models and signal analysis Grossmann and Morlet ((1984)); Mallat and Peyré ((2009)); Cohen ((2019)); Argoul and Le ((2003)); Le and Argoul ((2004)). These wavelets are defined by an order parameter which gives their number of vanishing moments and their number of oscillations.

Here we have used the Cauchy Paul wavelet (python package pycwt), with parameter $m \geq 0$, defined in the frequency domain as:

$$\hat{\psi}_m(f) = \frac{2^m}{\sqrt{m\,\Gamma(2m)}}\, f^m\, \exp(-f)\ , \quad f > 0\ , \tag{7}$$

$\Gamma(n+1) = n!$ with $\forall n \in \mathbb{N}$, and $\hat{\psi}_m = 0$ for $f \leq 0$, with admissibility coefficient $c_\psi = m^{-1}$. The normalization is chosen to conserve a unit L^2 norm: $\|\psi_m\|_2 = \|a^{\frac{1}{2}}\hat{\psi}_m(af)\|_2 = \|a^{-\frac{1}{2}}\psi_m(\frac{t-b}{a})\|_2 = 1$. Its mean frequency $\bar{f}_{\psi_m}$ for L_2 norm is $\bar{f}_{\psi_m} = m + \frac{1}{2}$. Its peak frequency $f^0_{\psi_m} = m$ corresponds to the maximum of $\hat{\psi}_m$. The mean and peak frequencies are slightly different, indicating the asymmetrical nature of the shape of $\hat{\psi}_m(f)$. The standard deviation Δf_{ψ_m} of $\hat{\psi}_m$ is then: $\Delta f_{\psi_m} = \frac{\sqrt{2m+1}}{2}$. And the quality factor Q of this wavelet increases with the parameter m:

$$Q = \frac{\bar{f}_{\psi_m}}{2\Delta f_{\psi_m}} = \frac{\sqrt{2m+1}}{2}\ . \tag{8}$$

2.3 Numerical signals generated by a VAR(3) model

The two-variable AR(3) model that we use to test the different granger causality computations is defined in two subsequent time intervals, where the dynamics of Y is changed:

$$X_t = a_{x,1}X_{t-1} + a_{x,2}X_{t-2} + a_{x,3}X_{t-3} + b_{xy,1}Y_{t-1} + b_{xy,2}Y_{t-2} + 0.5\varepsilon_{x,t} \quad (9)$$

$$Y_t = a_{y,1}X_{t-1} + a_{y,2}X_{t-2} + a_{y,3}X_{t-3} + b_{yx,1}X_{t-1} + b_{yx,2}X_{t-2} + \varepsilon_{y,t}\ , \quad (10)$$

for the first half of the whole time interval ($0 \leq t < 32767/200$ s), and

$$X_t = a_{x,1}X_{t-1} + a_{x,2}X_{t-2} + a_{x,3}X_{t-3} + b_{xy,1}Y_{t-1} + b_{xy,2}Y_{t-2} + 0.5\varepsilon_{x,t} \quad (11)$$

$$Y_t = a_{y,1}X_{t-1} + a_{y,2}X_{t-2} + a_{y,3}X_{t-3} + 2 * b_{yx,1}X_{t-1} + 2 * b_{yx,2}X_{t-2} + 0.5 * \varepsilon_{y,t}\ , \quad (12)$$

for the second half of the time interval ($32768/200 \leq t < 65536/200$ s).
with $a_{x,1} = 0.9$, $a_{x,2} = -0.6$, $a_{x,3} = 0$, $b_{xy,1} = 0$, $b_{xy,2} = 0$,
and $a_{y,1} = 0.8$, $a_{y,2} = -0.5$, $a_{y,3} = 0.3$, $b_{yx,1} = 2$, $b_{yx,2} = -0.4$.
$\varepsilon_{x,t}$ and $\varepsilon_{y,t}$ are two Gaussian white noise signals (generated by the python numpy.random.multivariate function) with covariance matrix $\begin{pmatrix} 1 & 0.4 \\ 0.1 & 3 \end{pmatrix}$

We show in Fig. 1 the plot of these two signals, their spectrograms and their Fourier spectra, computed either directly from the FFT algorithm or averaged from the modulus square of the wavelet transform. We took a frequency sampling of 200 Hz, to correspond precisely to the frequency sampling of the EEGs signals. We note that the signal X presents a wide frequency band centered around 30 Hz, on the opposite, the signal Y is rather flat, with no clear emerging peak.

Analytic results for this process can be deduced from the expression of the transfer function $\mathbf{H}(\omega)$ (causal factors):

$$\begin{pmatrix} \hat{X}(\omega) \\ \hat{Y}(\omega) \end{pmatrix} = \mathbf{H}(\omega) \begin{pmatrix} \hat{\varepsilon}_x(\omega) \\ \hat{\varepsilon}_y(\omega) \end{pmatrix} = \begin{pmatrix} 1-\mathcal{A}_x & -\mathcal{B}_{xy} \\ -\mathcal{B}_{yx} & 1-\mathcal{A}_y \end{pmatrix}^{-1} \begin{pmatrix} 0.5 & 0 \\ 0 & 1 \end{pmatrix} \begin{pmatrix} \hat{\varepsilon}_x(\omega) \\ \hat{\varepsilon}_y(\omega) \end{pmatrix} \quad (13)$$

$$= \frac{1}{C(\omega)} \begin{pmatrix} 0.5(1-\mathcal{A}_y) & \mathcal{B}_{xy} \\ 0.5(\mathcal{B}_{yx}) & 1-\mathcal{A}_x \end{pmatrix} \begin{pmatrix} \hat{\varepsilon}_x(\omega) \\ \hat{\varepsilon}_y(\omega) \end{pmatrix}$$

with $\mathcal{A}_x = a_{x,1}e^{i\omega} + a_{x,2}e^{i2\omega} + a_{x,3}e^{i3\omega}$, $\mathcal{A}_y = a_{y,1}e^{i\omega} + a_{y,2}e^{i2\omega} + a_{y,3}e^{i3\omega}$, $\mathcal{B}_{xy} = b_{xy,1}e^{i\omega} + b_{xy,2}e^{i2\omega}$, $\mathcal{B}_{yx} = b_{yx,1}e^{i\omega} + b_{yx,2}e^{i2\omega}$ and $C(\omega) = (1-\mathcal{A}_x)(1-\mathcal{A}y) - (\mathcal{B}_{xy})(\mathcal{B}_{yx})$.

What is added in your remark Alexandre? What do you mean with the equation eq:char-pol? $C(\omega) = \varphi_A(e^{i\omega})$ **from Eq. (??).**

3 GRANGER CAUSALITY AND ITS SPECTRAL FORMS

The concept of causality was elaborated by Granger from Wiener principles Granger ((1969, 1964)); Wiener and Masani ((1957)) on the assumption that the real signal x can be modeled by autoregressive equations of order p (AR(p)), that describes that the value observed at time t depends linearly on its own past values:

$$x_t = \sum_{k=1}^{p} a_k x_{t-k} + \epsilon_t, \quad (14)$$

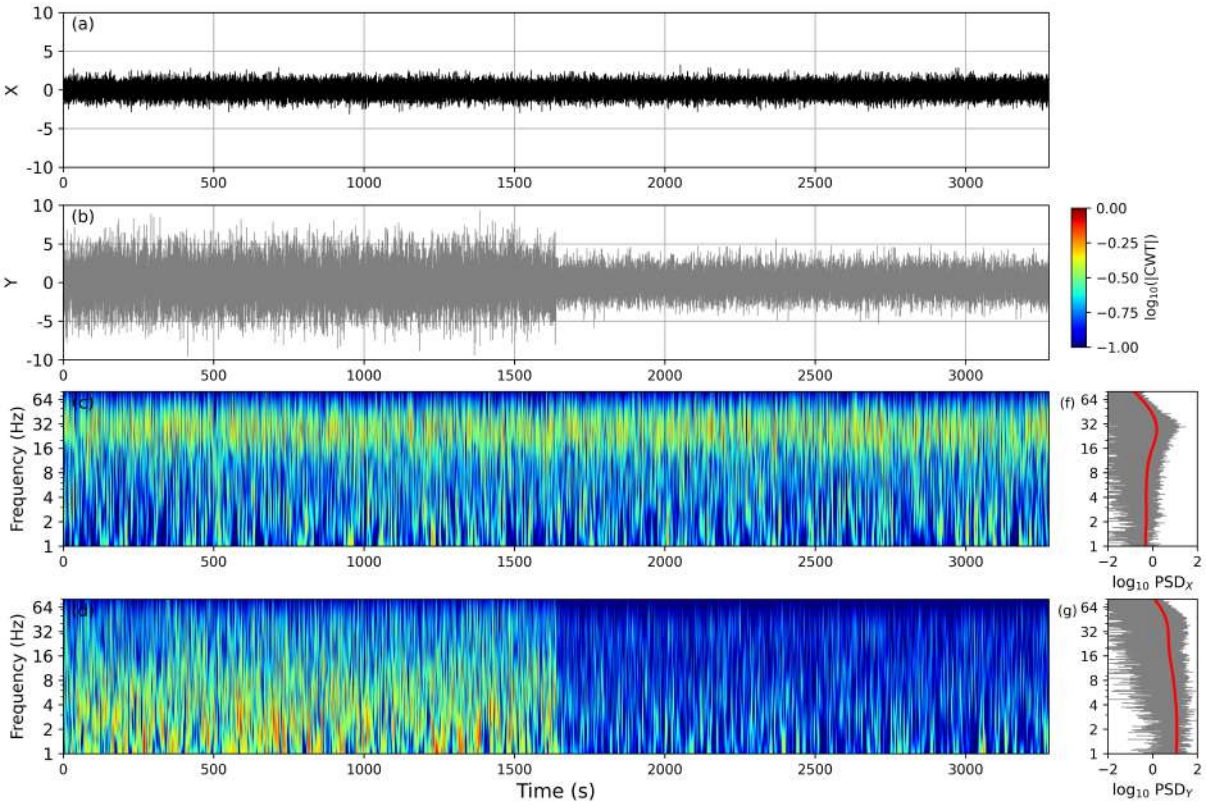

Figure 1. Two signals generated by the AR3 equations (Eqs (10) and (12)). (a) and (b) plots of $X(t)$ and $Y(t)$ respectively. (c) and (d) Modulus of the wavelet transform of X (c) and Y (d), coded in log-scale (see the color bar, on the right of (b)). (e) and (f): PSDs of X and Y (in log-scales) (grey lines) and the averaged PSDs computed from the mean of the modulus square of their wavelet transforms (Cauchy-Paul wavelet with $m = 4$), plotted in log-scales.

where a_k are the regression coefficients, and ϵ_t denotes the residual noise.

Most Granger causality approaches rely on the assumption that the system follows covariance stationarity, (or weak or wide-sense stationarity) and hence that its first moment and its covariance does not vary with time. Formally, a random process $\mathbf{X}_t$ is covariance stationary if it satisfies the restrictions on both its mean function:

$$\mathbb{E}[\mathbf{X}(t)] = m_{\mathbf{X}} \quad \forall t \in \mathbb{R}, \tag{15}$$

and its autocovariance function:

$$\mathbb{E}[(\mathbf{X}(t_1) - m_{\mathbf{X}})(\mathbf{X}(t_2) - m_{\mathbf{X}})] = C_{\mathbf{X}}(t_1, t_2) = C_{\mathbf{X}}(\tau), \quad \text{where } \tau = t_1 - t_2 \quad \forall t_1, t_2 \in \mathbb{R}\,. \tag{16}$$

[Bold notation for vector?]

3.1 Temporal (original Granger) causality

The definition of Granger causality relies on linear Gaussian autoregressive models, assumed to be Gaussian, homoscedastic and linear, which implies also stationary. Eq. (17) is written in the form of an

autoregressive model of order k (AR(k)) for the right hand side,

$$p_t(X_t|X_{t-1}^{t-k}) = \phi\left(X_t; \mu = \sum_{j=1}^{k} a_{x,j}^{(x)} X_{t-j}\ ,\ \sigma^2 = \Sigma_x^{(x)}\right)\ . \tag{17}$$

and Eq. (18) a vector autoregressive model of order k (VAR(k)) for the right-hand side:

$$p_t(X_t|X_{t-1}^{t-k}, Y_{t-1}^{t-k}) = \phi\left(X_t; \mu = \sum_{j=1}^{k} a_{xx,j}^{(yx)} X_{t-j} + \sum_{j=1}^{k} a_{xy,j}^{(xy)} Y_{t-j}\ ,\ \sigma^2 = \Sigma_{xx}^{(xy)}\right)\ . \tag{18}$$

ϕ represents the Gaussian probability density function. To test hypothesis of Eq. (17), GewekeGeweke ((1982, 1981)) proposed for Granger directional causality the ratio of residual variances $\Sigma_x^{(x)}$ and $\Sigma_{xx}^{(xy)}$:

$$F_{Y\to X} = \log\left(\frac{\Sigma_x^{(x)}}{\Sigma_{xx}^{(xy)}}\right) \tag{19}$$

Henceforth causality from Y to X implies an improvement in predictability of X when combining the past of X with that of Y, since the variance $\Sigma_{xx}^{(xy)}$ is reduced, compared to $\Sigma_x^{(x)}$. Similarly the Geweke measure of Granger directional causality from X to Y is defined:

$$F_{X\to Y} = \log\left(\frac{\Sigma_y^{(y)}}{\Sigma_{yy}^{(yx)}}\right) \tag{20}$$

Apart from these two directional measures of causality, Geweke proposed two other measures. A measure of instantaneous causality:

$$F_{X\cdot Y} = \log\left(\frac{\Sigma_{xx}^{(xy)}\Sigma_{yy}^{(xy)}}{|\Sigma^{(xy)}|}\right) \tag{21}$$

where $\Sigma^{(xy)}$ is the covariance matrix:

$$\Sigma^{(xy)} = \begin{pmatrix} \Sigma_{xx}^{(xy)} & \Sigma_{xy}^{(xy)} \\ \Sigma_{yx}^{(xy)} & \Sigma_{yy}^{(xy)} \end{pmatrix} \tag{22}$$

$F_{X\cdot Y}$ is zero for $\Sigma^{(xy)}$ diagonal. The fourth measure proposed by Geweke is the total dependence between X and Y Geweke ((1982)):

$$F_{X,Y} = \log\left(\frac{\Sigma_x^{(x)}\Sigma_y^{(y)}}{|\Sigma^{(xy)}|}\right) \tag{23}$$

This measure compares the prediction error within assumption of full independence of the two processes, and the prediction error of the bivariate projection, to account of any source of interdependence. With the last equation 24, Geweke highlighted that the total dependence of two processes X and Y depends both on directional causality and instantaneous interactions:

$$F_{X,Y} = F_{X\to Y} + F_{Y\to X} + F_{X\cdot Y} \tag{24}$$

In this study, we mainly use AR ($X_t \in \mathbb{R}$) and bivariate VAR ($X_t \in \mathbb{R}^2$) models to illustrate the computation of directional and instantaneous causality between pairs of physiological signals. The order k of the model for regression estimation of the residuals will be optimally chosen using standard information criteria (Akaike Information Criterion (AIC) and Bayesian Information Criterion (BIC) from python library statsmodels).

3.2 Geweke spectral formulation of Granger causality

Geweke Geweke ((1982)) proposed a spectral decomposition of the time-domain Granger causality measures with some strong requirements on the signals which can be found in Sup.Infos section 1.1 of this article.

Let us rewrite the matricial formulation of multivariated autoregressive (MVAR) processes:

$$\mathbf{X}_t = \mathbf{A}\mathbf{X}_{t-1}^{(p)} + \varepsilon_t = \sum_{k=1}^{p} A_k \mathbf{X}_{t-k} + \varepsilon_t \ , \tag{25}$$

where p is the model order, which may be infinite (under some hypothesis of convergence of the sum). The parameters of this model are the coefficients A_k ($\mathbf{A}$ is a $n \times m$ matrix), and the $n \times n$ residuals covariance matrix $\Sigma = \text{cov}(\varepsilon_t)$. By stationarity, the covariance matrix Σ does not depend on time. Geweke introducted a lag operator L such that

$$\mathbf{A}(L)\mathbf{X}_t = \varepsilon_t \tag{26}$$

with

$$\mathbf{A}(L) = I - \sum_{k=1}^{p} A_k L^K \ . \tag{27}$$

If we note $\mathbf{H}(L) = \mathbf{A}(L)^{-1}$, the recursion model 25 reads:

$$\mathbf{X}_t = \mathbf{H}(L)\varepsilon_t \ . \tag{28}$$

We can then transform this equation in the frequency domain via a discrete time series Fourier transform:$\mathbf{X}(\omega) = \sum_{t\to-\infty}^{\infty} \mathbf{X}_t e^{-i\omega t}$ and write $L = e^{-i\omega}$, we get the spectral formulation of the MVAR model (Eq. (25:

$$bfA(e^{-i\omega}).\mathbf{X}(\omega) = \mathbf{A}(\omega).\mathbf{X}(\omega) = \varepsilon(\omega) \tag{29}$$

Since we also have a corresponding transfer matrix: $\mathbf{H}(\omega) = \mathbf{A}(\omega)^{-1}$, we obtain:

$$\mathbf{X}(\omega) = \mathbf{H}(\omega)\epsilon(\omega) \tag{30}$$

In real data analysis, the range of ω values would be related to the sampling frequency f: $0 \leq \omega \leq 2\pi$, if we denote $\omega = 2\pi f/f_s = 2\pi f \delta t$.

The spectral densities matrices $\mathbf{S}(\omega)$ are $n \times n$ Hermitian positive semi-definite matrices. The inverse Fourier transform of $\mathbf{S}$ recovers the covariance matrix:

$$\mathbf{\Gamma}_k = \frac{1}{2\pi} \int_{-\pi}^{\pi} \mathbf{S}(\omega) e^{i\omega k} \mathrm{d}\omega \ \ , \ \ k = ..., -2, -1, 0, 1, 2, ... \tag{31}$$

Numerically, these Fourier series (or integrals) can be efficiently computed by Fast Fourier Transform (FFT) and inverse Fast Fourier Transform (iFFT).

The cross-spectral density matrix CPSD takes a matricial form:

$$\mathbf{S}(\omega) = \begin{pmatrix} S_{XX}(\omega) & S_{XY}(\omega) \\ S_{YX}(\omega) & S_{YY}(\omega) \end{pmatrix} \tag{32}$$

and we have similar decomposition for the transfer function $\mathbf{H}(\omega)$.

For a VAR process, the (CPSD) can be factorized Papoulis and Pillai ((2002)):

$$\mathbf{S}(\omega) = \mathbf{H}(\omega)\Sigma\ \mathbf{H}(\omega)^* \quad 0 \leq \omega \leq 2\pi \tag{33}$$

where the transfer function $H(\omega)$ is defined as the inverse matrix of the Fourier transfer of the regression coefficients:

$$\mathbf{H}(\omega) = \left(I - \sum_{k=1}^{p} A_k e^{-ik\omega} \right)^{-1} \qquad 0 \leq \omega \leq 2\pi\ . \tag{34}$$

Eq. 34 states that the VAR coefficients A_k may be recovered from $H(\omega)$ by a matrix inversion and inverse Fourier transform.

S_{XX} is just the CPSD of the sub-process $\mathbf{X}$ and from Eq. (33):

$$S_{XX}(\omega) = H_{XX}(\omega)\Sigma_{XX}H_{XX}(\omega)^* + 2\mathcal{R}(H_{XX}(\omega)\Sigma_{XY}H_{XY}(\omega)^*) + H_{XY}(\omega)\Sigma_{YY}H_{XY}(\omega)^* \tag{35}$$

Following Geweke Geweke ((1982)), in the special case $\Sigma_{XY} \equiv 0$, which may always be effected by a linear transformation of variables leaving $F_{Y\to X}$ invariant Barrett et al. ((2010)), $S_{XX}(\omega)$ takes the simple form:

$$S_{XX}(\omega) = H_{XX}(\omega)\Sigma_{XX}H_{XX}(\omega)^* + H_{XY}(\omega)\Sigma_{YY}H_{XY}(\omega)^* \tag{36}$$

whereby the CPSD of X splits into an "intrinsic" term and a "causal" term. This motivates the definition of the (unconditional) spectral G-causality from $\mathbf{Y}$ to $\mathbf{X}$ as:

$$\mathbf{f}_{\mathbf{Y}\to\mathbf{X}}(\omega) \equiv \log\left(\frac{|S_{XX}(\omega)|}{|S_{XX}(\omega) - H_{XY}\Sigma_{YY}H_{XY}(\omega)^*|} \right) \tag{37}$$

or, in terms of untransformed variables (i.e. where $\Sigma_{XY} \neq 0$),

$$\mathbf{f}_{\mathbf{Y}\to\mathbf{X}}(\omega) \equiv \log\left(\frac{|S_{XX}(\omega)|}{|S_{XX}(\omega) - H_{XY}\Sigma_{Y|X}H_{XY}(\omega)^*|} \right) \tag{38}$$

where the partial covariance matrix $\Sigma_{Y|X}$ is defined by:

$$\Sigma_{Y|X} = \Sigma_{YY} - \Sigma_{YX}\Sigma_{XX}^{-1}\Sigma_{XY}\ . \tag{39}$$

[??? je ne comprends pas ta remarque. If this is true, then the negative term is zero. Else, one of the above equation should be redefined.]

Geweke then established the fundamental spectral decomposition of G-causality in the unconditional case (which is almost always satisfied):

$$F_{Y\to X} = \frac{1}{2\pi}\int_0^{2\pi} \mathbf{f}_{\mathbf{Y}\to\mathbf{X}}(\omega)\mathrm{d}\omega \ , \tag{40}$$

so that time domain causality may be thought of as the average over all frequencies of spectral causality.

Geweke made further strong hypothesis for the frequency expression of $F_{X\to Y}$ and $F_{Y\to X}$, $f_{X\to Y}(\omega)$ and $f_{Y\to X}(\omega)$ if they exist, they should be nonnegative functions such that

$$F_{X\to Y} = \frac{1}{2\pi}\int_{-\infty}^{\infty} f_{X\to Y}(\omega)\mathrm{d}\omega \tag{41}$$

and

$$F_{Y\to X} = \frac{1}{2\pi}\int_{-\infty}^{\infty} f_{Y\to X}(\omega)\mathrm{d}\omega \tag{42}$$

The Geweke spectral causality Geweke ((1981, 1982)) allows us to identify, for each frequency band, the direction and intensity of interactions between signals. This approach is particularly relevant for EEG signals, whose dynamics are organised into distinct rhythms depending on the sleep phase. Note that this Geweke-Granger spectral factorization (which operates a kind of Hilbert transform) uses the full frequency range to compute the transfer functions, so that the influence of spectral modes on causality are not localized in time.

The instantaneous spectral causality can also be written from residual covariances between innovations of the two signals:

$$f_{X\cdot Y}(\omega) = \log\left(\frac{(H_{XX}(\omega)\Sigma_{YY}H_{XX}(\omega)^*)\cdot(H_{YY}(\omega)\Sigma_{XX}H_{YY}(\omega)^*)}{|S_{XX}(\omega)|}\right) \tag{43}$$

where $H_{XX}(\omega)$ and $H_{YY}(\omega)$ are the elements of the transfer function associated with each variable Geweke ((1982)).

Finally, total dependence at each frequency aggregates the directional and instantaneous effects:

$$f_{X,Y}(\omega) = f_{X\to Y}(\omega) + f_{Y\to X}(\omega) + f_{X\cdot Y}(\omega) \tag{44}$$

Frequency analysis thus adds an extra dimension to the study of causality: it allows us to quantify the directional influences between signals for each frequency band, and therefore to associate causal dynamics within specific physiological frequency bands. Furthermore, mathematical consistency between the temporal and frequency approaches is ensured: the integral of the spectral density of causality over all frequencies, normalised by 2π, gives exactly the temporal measure of Granger causality:

$$F_{Y\to X} = \frac{1}{2\pi}\int_{-\pi}^{\pi} f_{Y\to X}(\omega)\, d\omega \tag{45}$$

This fundamental property is demonstrated in Geweke ((1982)). This coupling between frequency reading and causal dynamics makes it possible to go beyond conventional power measurements to infer functional

relationships between the cortex and the autonomic system during sleep. Chicharro ((2011)); Ding et al. ((2006)); Shojaie and Fox ((2022)).

3.3 From spectral to time-frequency analysis of causality

[Notation problems.] As we have explained previously, Granger-Geweke spectral causality can be computed quite efficiently by transforming the VAR equations in frequency space by Fourier transform. Its generalization to time-frequency decomposition can be performed similarly, with wavelet time-frequency transform Dhamala et al. ((2008)).

Similar to the expression of $\mathbf{S}_{lm}(\omega)$ from the Fourier transforms of the signals $\mathbf{X}_l$ and $\mathbf{X}_m$: $\mathbf{S}_{lm}(\omega) = \mathbb{E}(\hat{\mathbf{X}}_l(\omega)\hat{\mathbf{X}}_m(\omega)^*)$, we write the time-frequency spectral density matrix:

$$\mathbf{S}_{lm}(t,\omega) = \mathbb{E}(\mathbf{W}_{X_l}(t,\omega)\mathbf{W}_{X_m}(t,\omega)^*) \ , \tag{46}$$

where ($l = 1, 2,\ m = 1, 2$) and $\mathbf{W}_X$ represents the time-frequency (wavelet) transform of $\mathbf{X}$ (based on sliding window Fourier decompositions). The average $\mathbb{E}$ is performed over multiple realizations. We will replace in the sequel the pulsation ω by the frequency f in Hz.

In the same line as Dhamala et al. ((2008)), we consider that the square time-frequency matrix $\mathbf{S}(t, f)$ can be defined in the interval $f = \omega f_s/2\pi \in [-f_s/2, f_s/2]$ and that it satisfies the following properties:

(i) $\mathbf{S}(t, f)$ is Hermitian, non-negative, and $\mathbf{S}(t, -f) = \mathbf{S}^T(t, f)$, where T denotes matrix transpose,

(ii) at each time, $\mathbf{S}(t, f)$ is integrable and can be Fourier transformed to get a covariance sequence matrix: $\gamma_{t,k} = \int_{-1/2}^{1/2} \mathbf{S}(t, f)e^{-ik2\pi f}\mathrm{d}f$, $k \in \mathbb{Z}$

[Notation: is there really the need for a covariance sequence here when based on wavelets?].

If we factorize this matrix $\mathbf{S}(t, f)$ at each time under the form of a product of two spectral minimum phase vectors $\chi(t, f)$ and its adjoint $\chi^*(t, f)$:

$$\mathbf{S}(t, f) = \chi(t, f)\chi(t, f)^* \tag{47}$$

with $\chi(t, f)$ a function of a complex variable $e^{i2\pi f}$, of generic form: $\chi(t, f) = \sum_{k=0}^{\infty} \mathbf{A}_{t,k}e^{ik2\pi f}$, defined in the unit circle and the matricial coefficients $\mathbf{A}_{t,k} = \int_{-1/2}^{1/2} \chi(t, f)e^{-ik2\pi f}\mathrm{d}f$. This Fourier decomposition is quite similar to that we have written for $\mathbf{S}(t, f)$. The factorization of $\mathbf{S}(t, f)$ into minimum-phase functions can be achieved with different algorithms Sayed and Kailath ((2001)), the method that we have selected for these computations is based on Cholesky decompositions (linalg package from scipy in python). If we rewrite equation 33 in time t and frequency f space:

$$\mathbf{S}(t, f) = \mathbf{H}(t, f)\mathbf{\Sigma}\mathbf{H}^*(t, f) \tag{48}$$

We remark that if we assume that at nul frequency the spectral density matrix can be identified with the Σ matrix:

$$\mathbf{\Sigma}(t) = \mathbf{A}_{t,0}\mathbf{A}_{t,0}^T \tag{49}$$

We can write Eq. 47 as:

$$\mathbf{S}(t, f) = \chi(t, f)\mathbf{A}_{t,0}^{-1}\mathbf{A}_{t,0}\mathbf{A}_{t,0}^T\mathbf{A}_{t,0}^{-T}\chi(t, f)^* \tag{50}$$

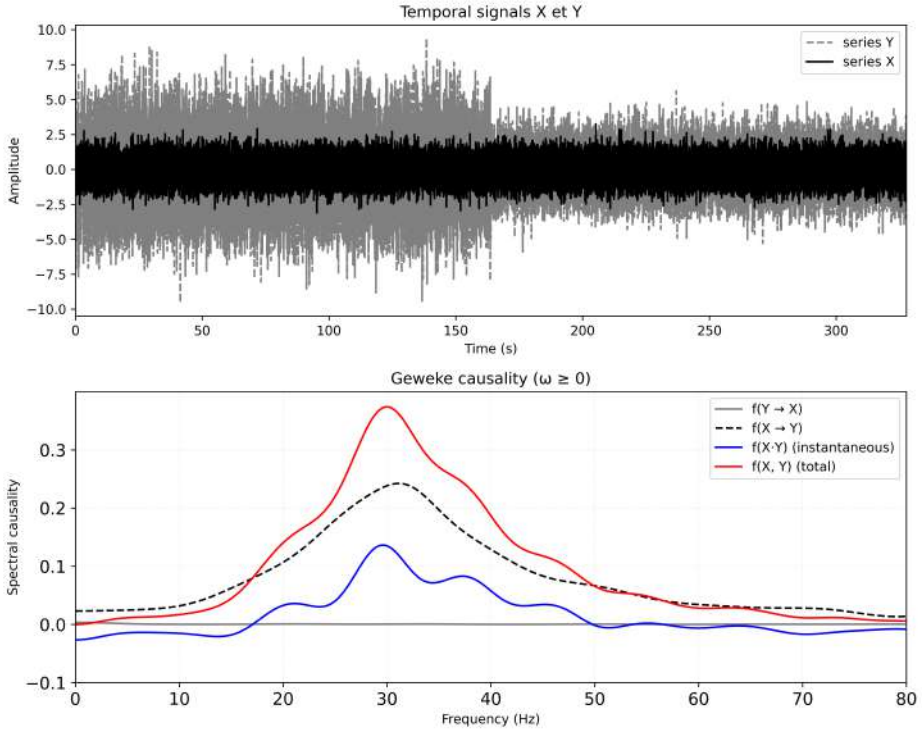

Figure 2. (a) 2 random signals X and Y generated by the VAR(3) model. (b) Spectral (Geweke) causality of X and Y. As expected the spectral causality $f_{X\to Y}$ remains nul. The integrals of these curves give the temporal Granger causality: $F_{Y\to X} \sim -7.10^{-5}$, $F_{X\to Y} \sim 0.06$, $F_{X.Y} \sim 0.01$, $F_{total} \sim 0.08$ [Analytic solution can be added using Eq. (13)] YES! I have the Granger temporal causality values also

and obtain a simple expression for the transfer function at each time t.

$$\mathbf{H}(t,f) = \chi(t,f)\mathbf{A}_{t,0}^{-1} \tag{51}$$

Then to estimate the time-frequency directional causalities, we simply replace the expressions of the matrix elements of $\mathbf{H}(\omega)$, $\mathbf{S}(\omega)$ and $\mathbf{\Sigma}$ into Eq.37

$$\mathbf{f_{Y\to X}}(t,f) \equiv \log\left(\frac{|S_{XX}(t,f)|}{|S_{XX}(t,f) - H_{XY}(t,f)\Sigma_{Y|X}H_{XY}(t,f)^*|}\right) . \tag{52}$$

4 RESULTS

We have implemented the different causality computations on two types of signals, respectively random signals generated by VAR(2) models, and EEG signals from the Physionet 2018 challenge (P2018C) Ghassemi et al. ((2018)); Goldberger et al. ((2000)).

4.1 Granger causality computations from model signals

For a more precise and reproducible comparison of the different methods previously proposed to compute the temporal, spectral and spectro-temporal causality, we first use model signals, generated by simple autoregressive models with additive noise (see Methods section).

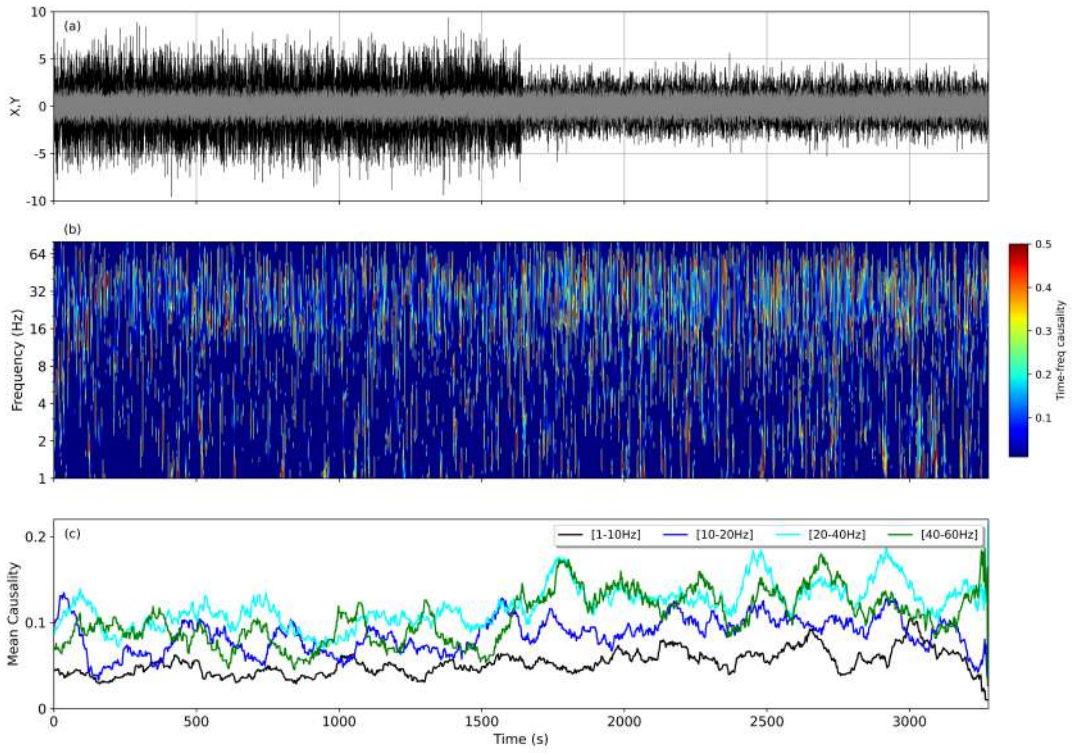

Figure 3. (a) Plots of signals $X(t)$ and $Y(t)$. (b) Causality scalogram (time-frequency wavelet transform). (c) Averaged causality computed from the causality scalogram in the frequency range $[30, 60]$ Hz. The red curve is computed from the average causality signal with a sliding window of 0.25s.

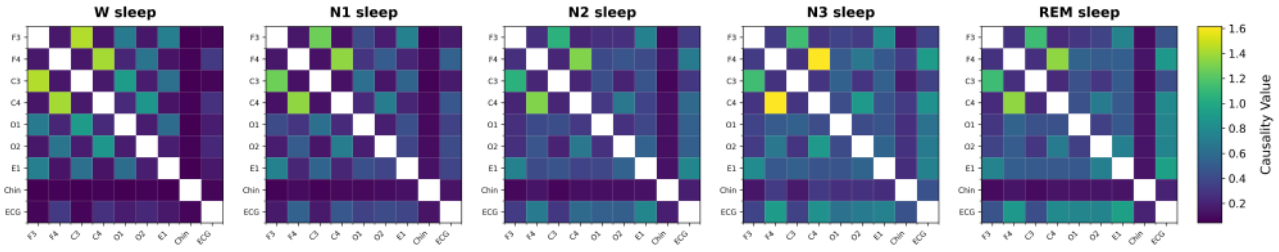

Figure 4. Causality matrices (global Granger causality) computed for the couples of signals of the tr03-0135 record of the P2018C. (attention le label du haut de cette figure doit etre corrige

4.2 Granger causality estimations from EEG signals

We have selected two EEGs signals recorded by polysomnography on one participant to the P2018C (tr03-0135). The EEGs correspond to the positions F4 and C4 respectively, which were selected after the construction of the causality matrices (Granger temporal estimated on epochs of ??? 30 s VERIFIER).

We have selected this couple ....

5 DISCUSSION AND PROSPECTIVES

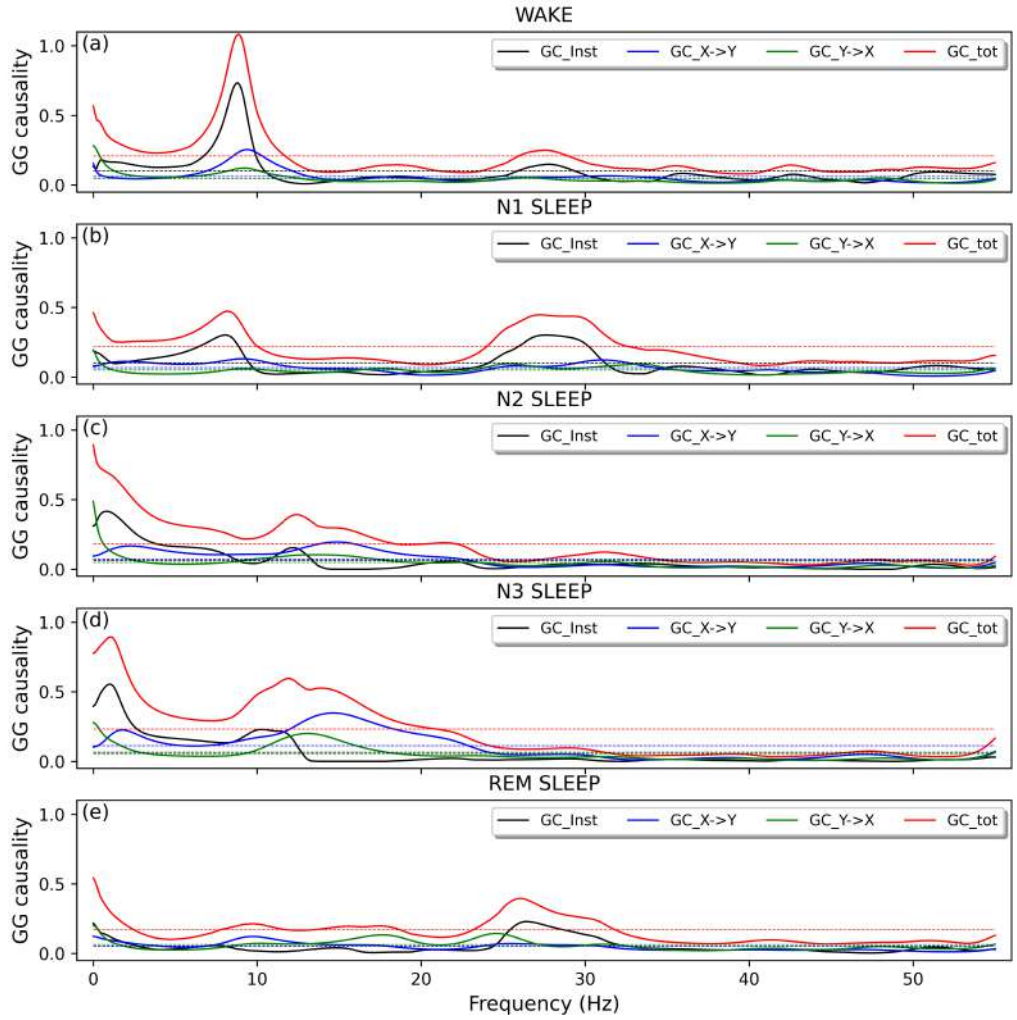

Figure 5. Geweke-Granger spectral causality computed with method I (section ...) from the tr03-0135 sample and the couple of cortex positions F4-F3.

6 APPENDIX

REFERENCES

C. L. Alves, T. G. L. D. O. Toutain, P. De Carvalho Aguiar, A. M. Pineda, K. Roster, C. Thielemann, J. A. M. Porto, and F. A. Rodrigues. Diagnosis of autism spectrum disorder based on functional brain networks and machine learning. *Scientific Reports*, 13(1):8072, May 2023. ISSN 2045-2322. doi: 10.1038/s41598-023-34650-6. URL https://www.nature.com/articles/s41598-023-34650-6.

P. Argoul and T.-P. Le. Instantaneous indicators of structural behavior based on the continuous Cauchy wavelet transform. *Mechanical Systems and Signal Processing*, 17:243–250, 2003.

L. A. Baccalá and K. Sameshima. Partial directed coherence: a new concept in neural structure determination. *Biological Cybernetics*, 84(6):463–474, May 2001. ISSN 0340-1200. doi: 10.1007/PL00007990. URL http://link.springer.com/10.1007/PL00007990.

A. B. Barrett, L. Barnett, and A. K. Seth. Multivariate Granger causality and generalized variance. *Physical Review E*, 81(4):041907, Apr. 2010. ISSN 1539-3755, 1550-2376. doi: 10.1103/PhysRevE.81.041907. URL https://link.aps.org/doi/10.1103/PhysRevE.81.041907.

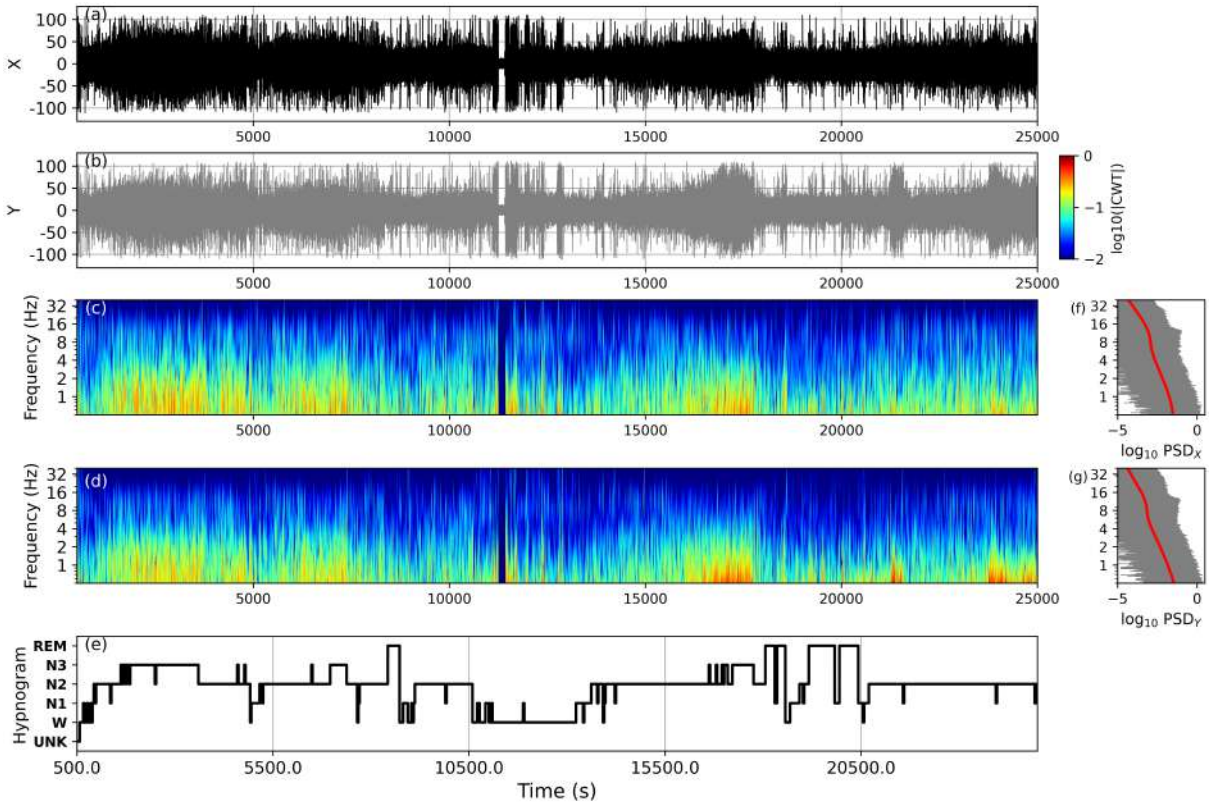

Figure 6. Two EEG signals, selected on cortex positions F4 and F3, from a patient of the P2018C database. (a) and (b) plots of $X(t)$ (F4) and $Y(t)$ (F3) respectively. (c) and (d) Modulus of the wavelet transform of X (c) and Y (d), coded in log-scale (see the color bar, on the right of (b)). (e) hypnogram. (f) and (g): PSDs of X and Y (grey lines) and the averaged spectra computed from the mean of the modulus square of the wavelet transform (red lines).

A. B. Barrett, M. Murphy, M.-A. Bruno, Q. Noirhomme, M. Boly, S. Laureys, and A. K. Seth. Granger Causality Analysis of Steady-State Electroencephalographic Signals during Propofol-Induced Anaesthesia. *PLoS ONE*, 7(1):e29072, Jan. 2012. ISSN 1932-6203. doi: 10.1371/journal.pone.0029072. URL https://dx.plos.org/10.1371/journal.pone.0029072.

R. Carmona, W. L. Hwang, and B. Torresani. Identification of Chirps with Continuous Wavelet Transform. In A. Antoniadis and G. Oppenheim, editors, *Wavelets and Statistics*, volume 103, pages 95–108. Springer New York, New York, NY, 1995. ISBN 978-0-387-94564-4 978-1-4612-2544-7.

R. Carmona, W. Hwang, and B. Torresani. Characterization of signals by the ridges of their wavelet transforms. *IEEE Transactions on Signal Processing*, 45 (10):2586–2590, 1997. ISSN 1053587X.

R. Carmona, W.-L. Hwang, and B. Torresani. *Practical time-frequency analysis: Gabor and wavelet transforms with an implementation in S*. Number v. 9 in Wavelet analysis and its applications. Academic Press, San Diego, 1998. ISBN 978-0-12-160170-6.

S. Charleston-Villalobos, M. Javorka, L. Faes, and A. Voss. Editorial: Granger causality and information transfer in physiological systems: basic research and applications. *Frontiers in Network Physiology*, 3:1284256, Oct. 2023. ISSN 2674-0109. doi: 10.3389/fnetp.2023.1284256. URL https://www.frontiersin.org/articles/10.3389/fnetp.2023.1284256/full.

D. Chicharro. On the spectral formulation of Granger causality. *Biological Cybernetics*, 105(5-6):331–347, Dec. 2011. ISSN 0340-1200, 1432-0770. doi: 10.1007/s00422-011-0469-z. URL http://link.springer.com/10.1007/s00422-011-0469-z.

M. X. Cohen. A better way to define and describe Morlet wavelets for time-frequency analysis. *NeuroImage*, 199:81–86, Oct. 2019. ISSN 10538119. doi: 10.1016/j.neuroimage.2019.05.048. URL https://linkinghub.elsevier.com/retrieve/pii/S1053811919304409.

M. Dhamala, G. Rangarajan, and M. Ding. Estimating Granger Causality from Fourier and Wavelet Transforms of Time Series Data. *Physical Review Letters*, 100(1):018701, Jan. 2008. ISSN 0031-9007, 1079-7114. doi: 10.1103/PhysRevLett.100.018701. URL https://link.aps.org/doi/10.1103/PhysRevLett.100.018701.

M. Ding, Y. Chen, and S. L. Bressler. Granger Causality: Basic Theory and Application to Neuroscience, Aug. 2006. URL http://arxiv.org/abs/q-bio/0608035. arXiv:q-bio/0608035.

P. Fries. A mechanism for cognitive dynamics: neuronal communication through neuronal coherence. *Trends in Cognitive Sciences*, 9(10):474–480, Oct. 2005. ISSN 13646613. doi: 10.1016/j.tics.2005.08.011. URL https://linkinghub.elsevier.com/retrieve/pii/S1364661305002421.

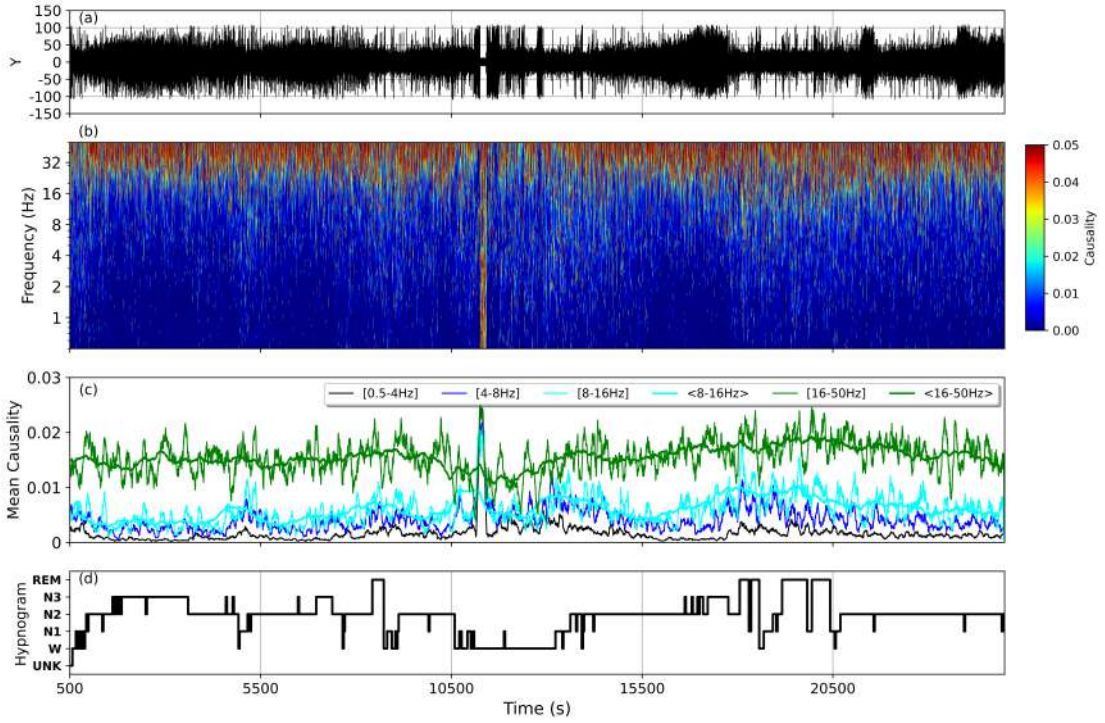

Figure 7. From the two EEG signals F4 and F3, for which we have computed the time-frequency spectrograms in Fig. 6, we computed the time-frequency(TF) causality. (a) plot of $Y(t)$ (F3). (b) Time frequency causality computed from the CWTs of X and Y with a Cauchy-Paul wavelet. (c) Averaged TF causality over windows of 0.25s or 2s (thicker lines), computed on different frequency bands (see legend). (d) Hypnogram.

J. Geweke. A Comparison of Tests of the Independence of Two Covariance-Stationary Time Series. *Journal of the American Statistical Association*, 76(374): 363–373, 1981.

J. Geweke. Measurement of Linear Dependence and Feedback Between Multiple Time Series. *Journal of the American Statistical Association*, 77(388): 304–313, 1982.

M. Ghassemi, B. Moody, L.-w. Lehman, C. Song, Q. Li, H. Sun, B. Westover, and G. Clifford. You Snooze, You Win: The PhysioNet/Computing in Cardiology Challenge 2018. Dec. 2018. doi: 10.22489/CinC.2018.049. URL http://www.cinc.org/archives/2018/pdf/CinC2018-049.pdf.

A. L. Goldberger, L. A. N. Amaral, L. Glass, J. M. Hausdorff, P. C. Ivanov, R. G. Mark, J. E. Mietus, G. B. Moody, C.-K. Peng, and H. E. Stanley. PhysioBank, PhysioToolkit, and PhysioNet: Components of a New Research Resource for Complex Physiologic Signals. *Circulation*, 101(23), June 2000. ISSN 0009-7322, 1524-4539. doi: 10.1161/01.cir.101.23.e215. URL https://www.ahajournals.org/doi/10.1161/01.CIR.101.23.e215. Publisher: Ovid Technologies (Wolters Kluwer Health).

C. W. J. Granger. *Spectral Analysis of Economic Time Series*. Princeton University Press, Princeton, N.J, 1964.

C. W. J. Granger. Investigating Causal Relations by Econometric Models and Cross-spectral Methods. *Econometrica*, 37(3):424–438, 1969.

A. Grossmann and J. Morlet. Decomposition of Hardy functions into square integrable wavelets of constant shape. *SIAM Journal on Mathematical Analysis*, 15 (4):723–736, 1984.

M. Havlicek, J. Jan, M. Brazdil, and V. D. Calhoun. Dynamic Granger causality based on Kalman filter for evaluation of functional network connectivity in fMRI data. *NeuroImage*, 53(1):65–77, Oct. 2010. ISSN 10538119. doi: 10.1016/j.neuroimage.2010.05.063. URL https://linkinghub.elsevier.com/retrieve/pii/S1053811910007962.

M. J. Kaminski and K. J. Blinowska. A new method of the description of the information flow in the brain structures. *Biological Cybernetics*, 65(3):203–210, July 1991. ISSN 0340-1200, 1432-0770. doi: 10.1007/BF00198091. URL http://link.springer.com/10.1007/BF00198091.

T.-P. Le and P. Argoul. Continuous wavelet transform for modal identification using free decay response. *Journal of Sound and Vibration*, 277(1-2):73–100, Oct. 2004. ISSN 0022460X. doi: 10.1016/j.jsv.2003.08.049. URL https://linkinghub.elsevier.com/retrieve/pii/S0022460X03012124.

W. Liao, D. Mantini, Z. Zhang, Z. Pan, J. Ding, Q. Gong, Y. Yang, and H. Chen. Evaluating the effective connectivity of resting state networks using conditional Granger causality. *Biological Cybernetics*, 102(1):57–69, Jan. 2010. ISSN 0340-1200, 1432-0770. doi: 10.1007/s00422-009-0350-5. URL http://link.springer.com/10.1007/s00422-009-0350-5.

M.-E. Lynall, D. S. Bassett, R. Kerwin, P. J. McKenna, M. Kitzbichler, U. Muller, and E. Bullmore. Functional Connectivity and Brain Networks in Schizophrenia. *Journal of Neuroscience*, 30(28):9477–9487, July 2010. ISSN 0270-6474, 1529-2401. doi: 10.1523/JNEUROSCI.0333-10.2010. URL https://www.jneurosci.org/lookup/doi/10.1523/JNEUROSCI.0333-10.2010.

S. G. Mallat and G. Peyré. *A wavelet tour of signal processing: the sparse way*. Elsevier [u.a.], Amsterdam, 3. ed edition, 2009. ISBN 978-0-12-374370-1.

A. Papoulis and S. U. Pillai. *Probability, random variables, and stochastic processes*. McGraw-Hill series in electrical and computer engineering. McGraw-Hill, Boston New Delhi, fourth edition edition, 2002. ISBN 978-0-07-366011-0 978-0-07-048658-4.

E. Piasini and S. Panzeri. Information Theory in Neuroscience. *Entropy*, 21(1):62, Jan. 2019. ISSN 1099-4300. doi: 10.3390/e21010062. URL https://www.mdpi.com/1099-4300/21/1/62.

D. L. Rocca, P. Campisi, B. Vegso, P. Cserti, G. Kozmann, F. Babiloni, and F. D. V. Fallani. Human brain distinctiveness based on EEG spectral coherence connectivity. *IEEE Transactions on Biomedical Engineering*, 61(9):2406–2412, Sept. 2014. ISSN 0018-9294, 1558-2531. doi: 10.1109/TBME.2014.2317881. URL http://arxiv.org/abs/1403.6384. arXiv:1403.6384 [q-bio].

A. H. Sayed and T. Kailath. A survey of spectral factorization methods. *Numerical Linear Algebra with Applications*, 8(6-7):467–496, Sept. 2001. ISSN 1070-5325, 1099-1506. doi: 10.1002/nla.250. URL https://onlinelibrary.wiley.com/doi/10.1002/nla.250. Publisher: Wiley.

T. Schreiber. Measuring Information Transfer. *Physical Review Letters*, 85(2):461–464, July 2000. ISSN 0031-9007, 1079-7114. doi: 10.1103/PhysRevLett.85.461. URL https://link.aps.org/doi/10.1103/PhysRevLett.85.461.

A. K. Seth, A. B. Barrett, and L. Barnett. Granger Causality Analysis in Neuroscience and Neuroimaging. *The Journal of Neuroscience*, 35(8):3293–3297, Feb. 2015. ISSN 0270-6474, 1529-2401. doi: 10.1523/JNEUROSCI.4399-14.2015. URL https://www.jneurosci.org/lookup/doi/10.1523/JNEUROSCI.4399-14.2015.

A. Shojaie and E. B. Fox. Granger Causality: A Review and Recent Advances. *Annual Review of Statistics and Its Application*, 9(1):289–319, Mar. 2022. ISSN 2326-8298, 2326-831X. doi: 10.1146/annurev-statistics-040120-010930. URL https://www.annualreviews.org/doi/10.1146/annurev-statistics-040120-010930.

B. Torresani and Y. Meyer, editors. *Analyse continue par ondelettes*. Savoirs actuels. Série physique. InterEditions, Paris, 1995. ISBN 978-2-7296-0591-9 978-2-7598-0264-7.

R. Vicente, M. Wibral, M. Lindner, and G. Pipa. Transfer entropy—a model-free measure of effective connectivity for the neurosciences. *Journal of Computational Neuroscience*, 30(1):45–67, Feb. 2011. ISSN 0929-5313, 1573-6873. doi: 10.1007/s10827-010-0262-3. URL http://link.springer.com/10.1007/s10827-010-0262-3.

N. Wiener and P. Masani. The prediction theory of multivariate stochastic processes. I. The regularity condition. *Acta Mathematica*, 98:111–150, 1957.